

# Crossover effects on the phase transitions phenomena translated by arborecences and spectral properties

Roberto da Silva

*Instituto de Física, Universidade Federal do Rio Grande do Sul, Porto Alegre Rio Grande do Sul, Brazil*

---

## Abstract

This study investigates how visibility graphs constructed from Monte Carlo Markov Chain time series of spin models capture the critical behavior of the system. More precisely, we show that this approach identifies continuous phase transitions as well as important nuances, such as crossover effects occurring in the transition from a critical line to a first-order line through a tricritical point, as observed, for example, in the Blume–Emery–Griffiths model or, in a simpler setting, in the Blume–Capel model. By applying Kirchhoff’s theorem, we show that the number of spanning trees of the resulting graphs serves as a sensitive indicator of these phase transitions. Furthermore, a qualitative analysis of the adjacency matrices based on random matrix theory provides additional evidence for these phenomena. The methodology developed here can potentially be extended to the analysis of criticality in empirical time series from complex systems, such as climate, financial, and epidemiological data, where the Hamiltonian governing the dynamics is not necessarily known.

---

## 1. Introduction

One important extension of the Ising model to spin  $S = 1$  variables is the well-known Blume–Emery–Griffiths (BEG) model [1], defined by the Hamiltonian

$$\mathcal{H} = -J \sum_{\langle ij \rangle} s_i s_j - K \sum_{\langle ij \rangle} s_i^2 s_j^2 + D \sum_i s_i^2, \quad s_i = 0, \pm 1, \quad (1)$$

or, in its simpler form, the Blume–Capel (BC) model [2, 3], which is obtained from the BEG Hamiltonian by setting  $K = 0$ ,

$$\mathcal{H}_{\text{BC}} = -J \sum_{\langle ij \rangle} s_i s_j + D \sum_i s_i^2. \quad (2)$$

Here,  $J$  denotes the bilinear exchange coupling,  $K$  the biquadratic interaction, and  $D$  the crystal-field term, which controls the population of non-magnetic states  $s_i = 0$ .

Originally introduced to describe phase separation and superfluid ordering in  $^3\text{He}$ – $^4\text{He}$  mixtures, the BEG model has since become a paradigmatic framework for the investigation of tricritical phenomena. In two dimensions, it exhibits a rich phase diagram comprising continuous phase

transitions in the Ising universality class, first-order transition lines, and a tricritical point separating these two regimes [4, 5]. The coexistence of multiple relevant couplings enhances crossover effects, which become particularly pronounced in both analytical approaches and numerical simulations.

For moderate values of  $D/J$  and  $K/J$ , the transition between the paramagnetic and ferromagnetic phases is continuous and governed by the two-dimensional Ising fixed point, characterized by the critical exponents  $\nu = 1$ ,  $\beta = \frac{1}{8}$ , and  $\alpha = 0$ . As the parameters are varied, this critical line terminates at a tricritical point, beyond which the transition becomes first order. At tricriticality, the critical behavior is described by a distinct set of exponents,  $\nu_t = \frac{5}{9}$ ,  $\beta_t = \frac{1}{24}$ , and  $\alpha_t = \frac{8}{9}$ , reflecting the presence of an additional relevant scaling field [4].

The crystal-field parameter  $D$  plays a central role in the crossover properties of the BEG model. Large negative values of  $D$  energetically suppress the  $s_i = 0$  state, effectively reducing the system to the standard spin- $\frac{1}{2}$  Ising model. In contrast, large positive values of  $D$  favor non-magnetic sites, leading to a strongly diluted magnetic system. In two dimensions, this continuous variation in the density of magnetically active spins induces a crossover between an Ising-like regime and a lattice-gas-like diluted regime, thereby modifying the structure of thermodynamic singularities such as the specific heat and susceptibility. This density-driven crossover significantly complicates the numerical identification of the true asymptotic critical behavior.

The proximity of the tricritical point leads to strong crossover effects. In renormalization-group language, the parameter space of the BEG model contains both an Ising fixed point and a tricritical fixed point, the latter possessing more than one relevant direction. As a consequence, the effective critical behavior observed depends on the length scale under consideration.

A characteristic crossover length

$$\xi_x \sim |g|^{-1/\phi} \quad (3)$$

separates the Ising-dominated regime from the tricritical one, where  $g$  measures the distance from the tricritical point and  $\phi$  is the crossover exponent [6]. For correlation lengths  $\xi \ll \xi_x$ , the system exhibits effective Ising-like critical behavior, whereas for  $\xi \gg \xi_x$  the tricritical scaling regime becomes dominant. In finite systems, or in simulations performed at parameters not asymptotically close to criticality, this mechanism naturally leads to effective critical exponents that interpolate between the Ising and tricritical values. Such crossover effects can also be systematically investigated within the simpler BC model.

Such crossover effects can alternatively be investigated using time-dependent Monte Carlo (MC) simulations, where critical parameters and exponents are extracted from the early stages of time evolution for both short-range and long-range (mean-field) interactions in two and three dimensions [7, 8, 9]. By focusing on short-time dynamics, universal critical behavior can be accessed without requiring full equilibration. Incorporating concepts from random matrix theory further allows for a spectral characterization of criticality. We have recently shown that matrices constructed from a small number of MC steps, within the framework of Wishart ensembles, encode the critical behavior of spin systems in their spectral properties [10, 11]. The same approach has been applied along the critical line of the BC model; however, its ability to accurately determine critical points becomes significantly affected near the tricritical point, reflecting the influence of crossover phenomena [12].

The idea of constructing matrices from time series of physical observables, such as the magnetization, whose spectra reflect the critical properties of the underlying system, naturally opens the door to the use of further concepts from the literature. One particularly appealing framework is the visibility graph (VG), which maps time series into graphs [13], thereby enabling the application of complex network theory to the investigation of temporal patterns with conceptual simplicity and strong physical interpretability. In the visibility algorithm introduced by Lacasa *et al.* [13], each data point  $(t_i, x_{t_i})$  is represented as a node  $i$ , and two nodes  $i$  and  $j$  are connected if a straight line drawn between  $(t_i, x_{t_i})$  and  $(t_j, x_{t_j})$  does not intersect any intermediate data point. This construction allows one to quantify temporal complexity topologically and to extract scaling properties directly from the network structure.

Time series generated by spin models have already been explored within this framework. For instance, Zhao *et al.* [14] investigated networks constructed from Ising model time series, while Gomez-Hernandez *et al.* [15] demonstrated that networks built from time series of both Ising and Kuramoto models retain the ability to detect phase transitions. Similar analyses were reported by Moraes and Ferreira [16] for the contact process. However, these studies did not explore the spectral properties of random matrices associated with the adjacency matrices, nor did they address a central question of the present work: what can the number of spanning trees of graphs (or equivalently its logarithm, the so-called structural entropy), constructed from distinct MC evolutions of spin systems governed by the standard Metropolis MCMC dynamics, reveal about phase transitions?

This idea was recently proposed by us in the context of the Ising model [17]. In the present work, we extend and refine this method to investigate the critical line of the BC model and its associated crossover phenomena. In particular, we analyze both the structural entropy—defined as the logarithm of any cofactor of the Laplacian matrix, since all cofactors are identical according to Kirchhoff’s theorem—and the eigenvalue density and level-spacing distribution of the adjacency matrix spectrum.

The remainder of this paper is organized as follows. In the next section, we describe the methodology. Section 3 presents the main results, and Sec. 4 summarizes the conclusions.

## 2. Methodology

We evolve the BC model using the heat-bath dynamics starting from a random initial magnetization ( $m_0 \approx 0$  in general, or other value when mentioned). Let us define

$$m_{i,j} = \frac{1}{L^2} \sum_{k=1}^{L^2} s_k^{(i,j)} \quad (4)$$

as the magnetization per spin at the  $i$ -th MC step ( $i = 0, 1, 2, \dots, N_{\text{steps}} - 1$ ) of the  $j$ -th independent run ( $j = 1, \dots, N_{\text{run}}$ ). Here, the spin variables  $s_k^{(i,j)} = 0, \pm 1$ . Thus, we can construct the VG for the  $j$ -th evolution, represented by the time series  $m_{0j}, m_{1j}, \dots, m_{N_{\text{steps}}-1,j}$ . The adjacency matrix of the VG is defined by representing each data point  $(i, m_{i,j})$  in the time series as a node  $i$ . Two nodes  $i$  and  $i'$  are said to be adjacent (or connected) if a straight line can be drawn between the points

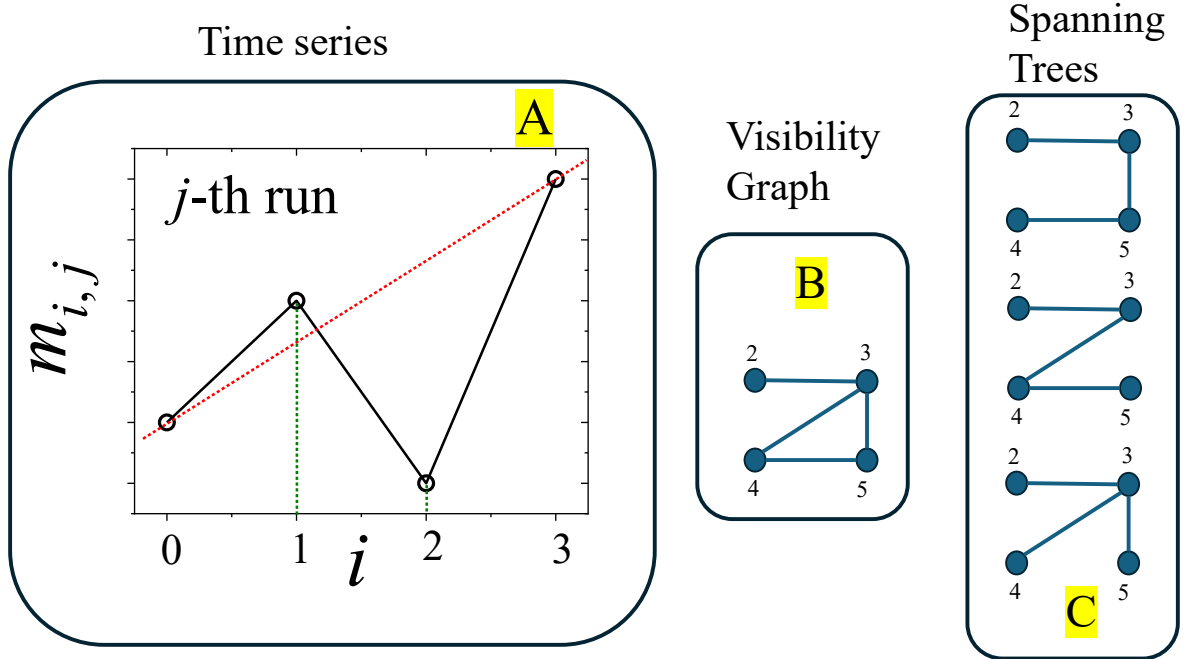


Figure 1: **Plot A**: A possible time evolution ( $j$ -th evolution) of the magnetization of the BC model for  $N_{\text{steps}} = 4$ . **Plot B**: Visibility graph corresponding to the time series. **Plot C**: All spanning trees of the visibility graph.

$(i, m_{i,j})$  and  $(i', m_{i',j})$  without intersecting any intermediate points. A simple illustration is shown for the case of Fig. 1.

Here we consider one arbitrary case with  $N_{\text{steps}} = 4$ . The Plot A illustrates the time evolution of magnetization for one run ( $j$ -th for the example). Following the rule, node 0 is visible by 1. 1 is visible obviously by node 0 and by nodes 2 and 3. Finally, the node 3 is visible only by 2 and 1. The resulting visibility graph is shown in Plot B. One of most important concepts of this paper is of spanning tree. Given a graph, a spanning tree is a connected subgraph that includes all the nodes of the original graph and contains no cycles. Trees, are in a general way a simpler form to cover nodes of a way where all nodes are reachable for the other ones without redundances. The number of spanning trees of a connected graph  $G$ , denoted by  $\tau(G)$ , is a fundamental combinatorial quantity that appears in a wide range of theoretical contexts (see for example [18, 19, 20]).

A classical physical interpretation of  $\tau(G)$  arises from its analogy with electrical resistor networks, first established by Kirchhoff [21] in his pioneering work. Since simple graphs – such as the VG – are fully characterized by their (symmetric) adjacency matrix  $A$ , whose elements satisfy  $a_{ij} = 1$  if nodes  $i$  and  $j$  are connected and  $a_{ij} = 0$  otherwise, Kirchhoff formulated a fundamental result known as the *Matrix-Tree Theorem* (see, for example, [22]).

Given a connected graph  $G$  (as is the case for VGs by construction) with adjacency matrix  $A$ , one can define another fundamental matrix: the Laplacian matrix, given by

$$L = -A + D,$$

where  $D$  is the diagonal matrix whose elements are given by  $D_{ii} = \sum_{j=1}^{N_{\text{steps}}} a_{ij}$ . By definition,  $a_{ii} = 0$ . All cofactors of the Laplacian matrix  $L$  are equal, and each of them corresponds to the number of spanning trees of the graph  $G$ . For simplicity, we select the first cofactor, which yields

$$\tau(G) = \det(L') = \prod_{i=1}^{N_{\text{steps}}-1} \lambda_i(L'), \quad (5)$$

where  $L'$  is the matrix obtained from  $L$  by removing its first row and first column. Its elements can be written as:

$$L'_{ij} = \begin{cases} \sum_{k=1}^{N_{\text{steps}}} a_{i+1,k}, & \text{if } i = j, \\ -a_{i+1,j+1}, & \text{otherwise,} \end{cases}$$

and  $\lambda_1, \lambda_2, \dots, \lambda_{N_{\text{steps}}-1}$  denote the eigenvalues of  $L'$ .

Referring to Fig. 1, let us clarify this point in a pedagogical manner by explicitly examining the adjacency matrix of the graph shown in Plot B and its corresponding Laplacian matrix:

$$A = \begin{pmatrix} 0 & 1 & 0 & 0 \\ 1 & 0 & 1 & 1 \\ 0 & 1 & 0 & 1 \\ 0 & 1 & 1 & 0 \end{pmatrix}, L = \begin{pmatrix} 1 & -1 & 0 & 0 \\ -1 & 3 & -1 & -1 \\ 0 & -1 & 2 & -1 \\ 0 & -1 & -1 & 2 \end{pmatrix}, \text{ and } L' = \begin{pmatrix} 3 & -1 & -1 \\ -1 & 2 & -1 \\ -1 & -1 & 2 \end{pmatrix}$$

We observe that the determinant of  $L'$  is equal to 3, which is naturally consistent with its eigenvalues,  $\lambda_1 = \sqrt{3} + 2$ ,  $\lambda_2 = 2 - \sqrt{3}$ , and  $\lambda_3 = 3$ , since  $\lambda_1 \lambda_2 \lambda_3 = 3$ . Therefore, the graph has exactly three distinct spanning trees, which are shown in Plot C of Fig. 1.

An important observation is that, if we consider the eigenvalues of the Laplacian matrix  $L$  (rather than those of the reduced matrix  $L'$ ), denoted by  $\xi_1, \xi_2, \dots, \xi_{N_{\text{steps}}}$ , then necessarily  $\xi_1 = 0$ , while all the remaining eigenvalues are strictly positive, provided the graph is connected. In this case, one can show that:

$$\tau(G) = \frac{1}{N_{\text{steps}}} \prod_{i=2}^{N_{\text{steps}}} \xi_i(L) \quad (6)$$

and in this case you do not think in cofactors to calculate  $\tau(G)$ , but it is only an alternative and both directions (Eqs. 5 and 6) are valid as you want.

Within this approach, the computation of cofactors becomes unnecessary for evaluating  $\tau(G)$ . This representation is merely an alternative formulation, and both expressions (Eqs. 5 and 6) are mathematically equivalent and can be employed according to convenience.

Having illustrated the method with this simple example, we now turn to the more general case that will be addressed throughout this manuscript: a longer magnetization time series. In this scenario, the adjacency matrix  $A$  of the associated time VG can be written, in general form, as

$$a_{i,i'} = \prod_{k=i+1}^{i'-1} H \left( m_{i,j} + (m_{i',j} - m_{i,j}) \cdot \frac{(k-i)}{(i'-i)} - m_{k,j} \right)$$

where  $H(x)$  is the Heaviside step function:

$$H(x) = \begin{cases} 0 & \text{if } x < 0 \\ 1 & \text{if } x \geq 0. \end{cases}$$

In other words, for node  $i$  to be adjacent to node  $i'$ , it is necessary that  $H = 1$  for all  $k$  in the interval  $i + 1 \leq k \leq i' - 1$ . The matrix  $A$  is therefore a binary, symmetric matrix with a null diagonal.

At first glance, one might be tempted to argue that VGs constructed from magnetization time series at high temperatures should resemble random graphs. In the high-temperature regime, the magnetization behaves approximately as non-correlated Gaussian noise, and one could naively expect that the associated adjacency matrices would share properties with symmetric random matrices. In classical random graph models, two nodes  $i$  and  $j$  are connected independently with probability  $p$ , and disconnected with probability  $1 - p$ . In suitable limits, the spectral properties of such matrices may approach those described by the Gaussian Orthogonal Ensemble (GOE), including the emergence of the Wigner semicircle law (or controlled deviations from it) for the eigenvalue density.

However, this reasoning is incorrect in the present context. Even if the magnetization time series becomes Gaussian at high temperatures, the corresponding VG is not a random graph in the Erdős–Rényi sense. The crucial difference lies in the construction rule: edges in a VG are not assigned independently with a fixed probability, but are determined by deterministic geometric constraints imposed by the time series. As a consequence, the entries of  $A$  are strongly correlated, and the resulting network ensemble is structurally distinct from classical random graph ensembles.

This distinction is essential. The eigenvalue density and level spacing distribution of adjacency matrices derived from VGs should not be directly compared with GOE predictions at any temperature. Instead, an appropriate reference must be built from visibility graphs generated from Gaussian noise itself, preserving the same construction mechanism. In the next section, we present our results.

### 3. Results

Thus, we perform MC simulations of the two-dimensional BC model using heat-bath dynamics. The system is evolved for  $N_{\text{steps}} = 100$  time steps, starting from initial conditions with  $m_0 \approx 0$  (except in cases where other initial conditions are explicitly specified), for each value of  $D$ . Each evolution is repeated over  $N_{\text{run}} = 10^5$  independent runs.

For every run, the resulting time series generates a VG with  $N_{\text{steps}} = 100$  nodes, together with its corresponding adjacency and Laplacian matrices. This procedure yields  $10^7$  eigenvalues for the estimation of the eigenvalue density and  $10^5$  different values of the number of spanning trees, allowing a reliable average for estimating the structural entropy per node, or simply the tree

$D_C$	0	1	1.5	1.9501	1.9655
$T_C$	1.695	1.398	1.150	0.650	0.610

Table 1: Critical points of BC model chosen to be studied in this work. For reference see for example [23, 24].

entropy, defined as [17]

$$s = \lim_{N_{\text{run}} \rightarrow \infty, N_{\text{steps}} \rightarrow \infty} \frac{1}{N_{\text{steps}} N_{\text{run}}} \sum_{i=1}^{N_{\text{run}}} \ln \tau(G_i).$$

We considered five different values of  $D/J$  in our simulations: 0, 1, and 1.5, which are points far from the tricritical point, as well as  $D/J = 1.9501$  and the tricritical point itself,  $D/J = 1.9655$ . These values are listed in Table 1 (see [23, 24]).

For simplicity, in tables and plots we use  $D$  instead of  $D/J$ , which is equivalent to setting  $J = 1$  without loss of generality.

Thus, we divide our results into two parts. The first part concerns the Laplacian matrix, where we compute the number of spanning trees of the VGs constructed from the magnetization time evolutions of the BC model. The second part consists of a random matrix analysis of the adjacency matrix of the corresponding VGs. Although this second approach does not provide a direct method to locate the critical points, as the first one does, it offers useful supporting insights, particularly through the study of crossover effects and through the characterization of the low- and high-temperature regimes revealed by the VGs.

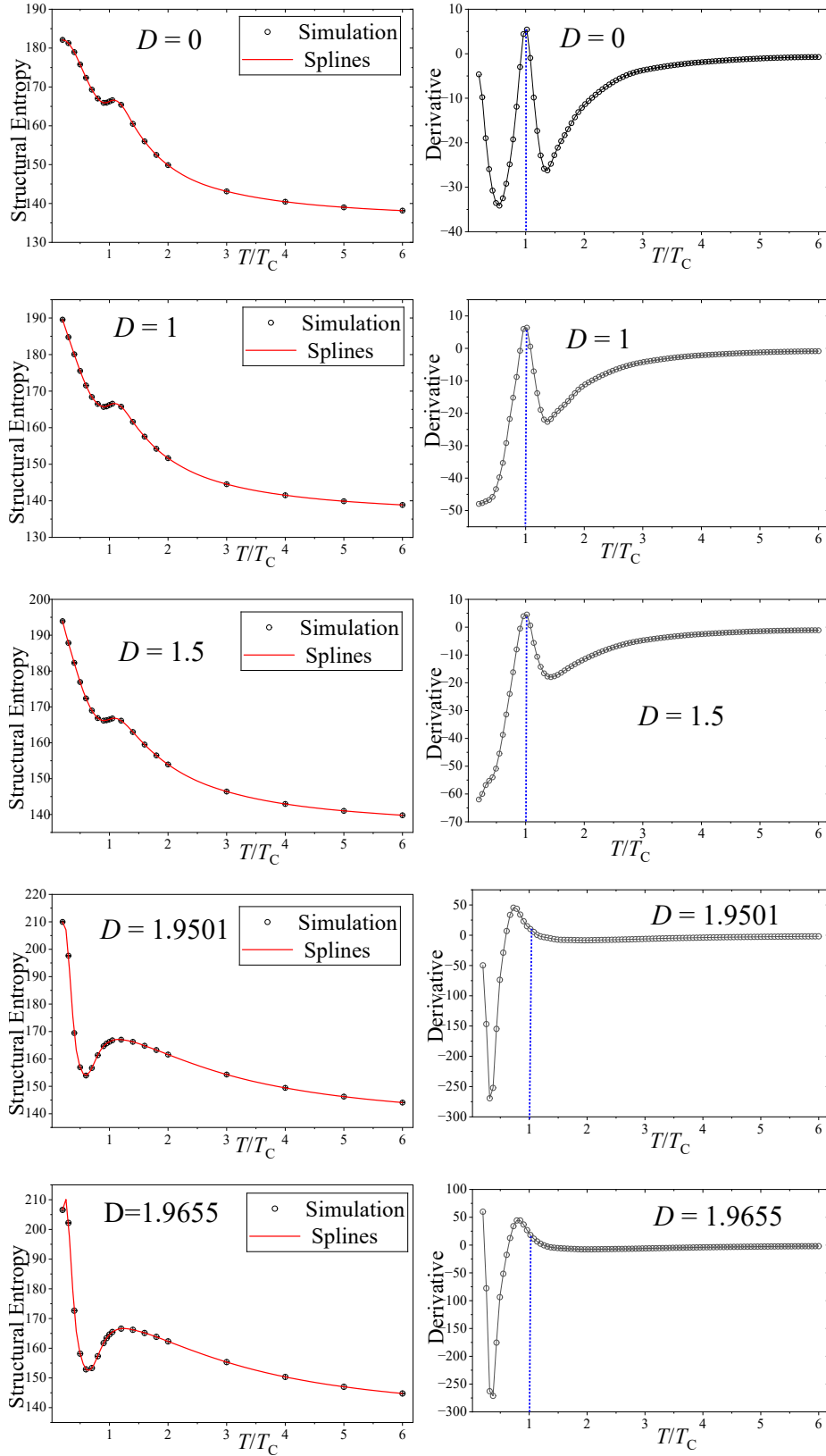
### 3.1. Laplacian matrix results

We begin by presenting the structural entropy, estimated as  $S = N_{\text{steps}} s = \frac{1}{N_{\text{run}}} \sum_{i=1}^{N_{\text{run}}} \ln \tau(G_i)$ , as a function of  $T/T_C$ . In Fig. 2 we show the structural entropy (left panels) together with its derivative (right panels) for the different values of  $D$  (see Table 1). The red curve corresponds to a spline interpolation included only as a guide to the eye.

In the left panels, a small plateau around  $T/T_C = 1$  can be observed for the first three values ( $D = 0, 1, \text{ and } 1.5$ ), since these points are far from the tricritical region and therefore do not exhibit significant crossover effects. In the corresponding right panels, the derivative of this quantity consistently exhibits a peak at the critical temperature, as also observed for the spin-1/2 Ising model [17]. However, these peaks do not coincide with  $T/T_C = 1$  for  $D = 1.9501$ , which is close to the tricritical point, nor for the tricritical point itself ( $D = 1.9655$ ), illustrating that crossover effects affect the estimates, as expected.

Following our analysis, it is important to emphasize that the tree entropy does not exhibit a maximum at the critical temperature; instead, the maximum appears in its derivative. However, as observed for the spin-1/2 Ising model [17], a maximum occurs near  $T = T_C$  when  $m_0 \neq 0$ . When  $m_0$  becomes sufficiently small, this peak gradually transforms into a plateau that contains  $T = T_C$ . The same behavior is observed here for the critical points of the BC model with different anisotropies.

To illustrate this effect, we show the evolution of the peak as a function of  $m_0$ . For simplicity, we present the case  $D = 1$ , since the other cases behave similarly, displaying the structural entropy



8

Figure 2: Structural entropy and its derivative as a function of  $T/T_C$  for different points along the critical line of the BC model. The tree entropy (structural entropy) exhibits a plateau in the vicinity of the critical temperature. In contrast, the derivative of this quantity shows a pronounced peak at  $T = T_C$  for points far from the tricritical point. In the vicinity of the tricritical point ( $D_C = 1.9501$ ) and at the tricritical point itself ( $D_C = 1.9655$ ), crossover effects affect the estimates, as expected.

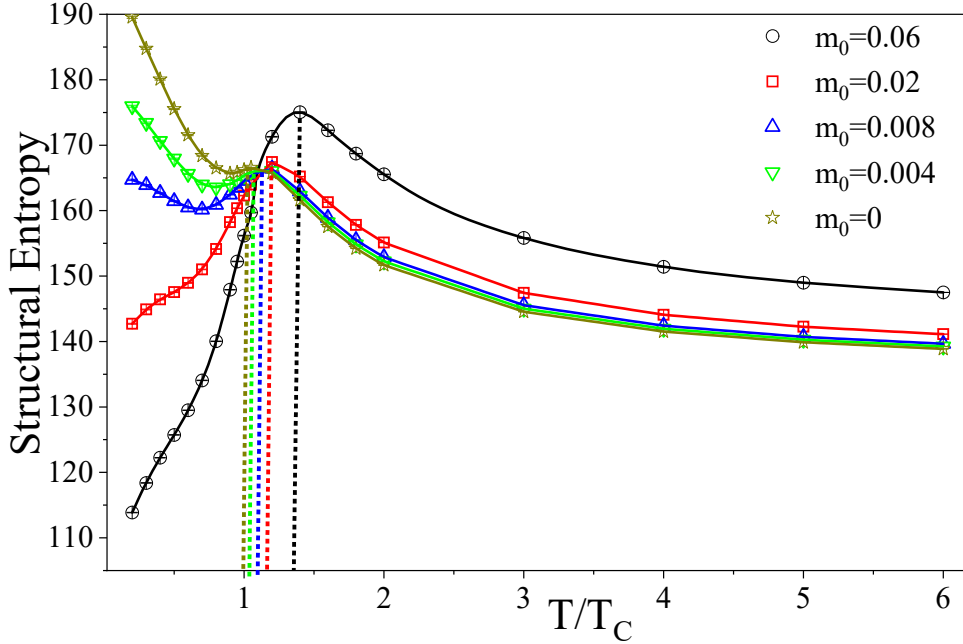


Figure 3: Effects of the initial conditions on the tree entropy. As  $m_0 \rightarrow 0$ , the peak gradually transforms into a plateau that includes the value  $T = T_C$ .

for  $m_0 = 0.06, 0.02, 0.008$ , and  $0.004$  (see Fig. 3). One can observe that the entropy exhibits a maximum at  $\tau^* = T^*/T_C$ ; however, this maximum does not coincide with  $\tau = 1$  when  $m_0 \neq 0$ . On the other hand, As  $m_0 \rightarrow 0$ , the peak gradually transforms into a plateau that includes the value  $T = T_C$ , by showing that the phenomenon should correspond to a maximum-entropy behavior, although with a more complex explanation. For clarity, we use  $\tau$  and  $T/T_C$  interchangeably in this work, since both denote the same quantity.

It is important to refine the plateau region. By zooming into this part of the figure, we obtain the behavior shown in Fig. 4(a), which reveals a sigmoidal dependence of the entropy as a function of  $\tau$ . This suggests that it is natural to perform a fit using a Boltzmann function:

$$S = \frac{A_1 - A_2}{1 + e^{\frac{(\tau - \tau_C)}{\sigma_\tau}}} + A_2,$$

as illustrated in the inset of Fig. 4(a).

It is useful to clarify the meaning of the fitting parameters. The constants  $A_1$  and  $A_2$  represent the asymptotic values of  $S$  in the two limiting regimes:  $A_1$  corresponds to the asymptotic value for  $\tau \ll \tau_C$  (initial plateau), whereas  $A_2$  corresponds to the asymptotic value for  $\tau \gg \tau_C$  (final plateau). The parameter  $\sigma_\tau$  represents the transition width, characterizing how abruptly the system changes between the two regimes. Finally,  $\tau_C$  indicates the location of the transition between these regimes.

It is important to note that for  $\tau = \tau_C$  one obtains  $S(\tau = \tau_C) = \frac{A_1 + A_2}{2}$ , and the maximal slope

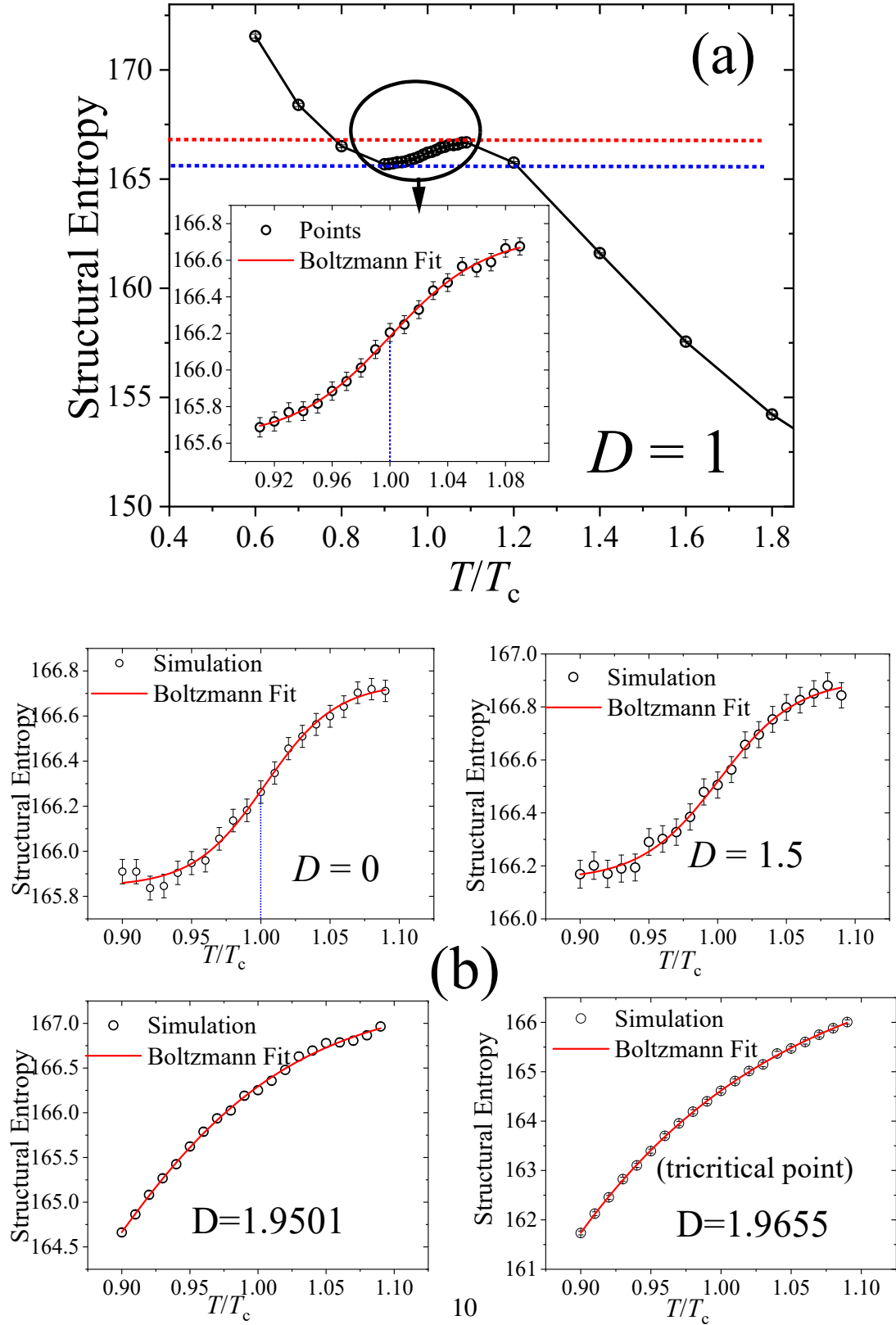


Figure 4: (a) Zoom of the plateau region for the case  $D = 1$ . This region is well described by a Boltzmann (sigmoidal) function. (b) Boltzmann fits for the other values of  $D$ . The tricritical point and the nearby point are not well fitted due to crossover effects, which are characterized by the parameter  $x_0$ .

$D_C$	$\tau_C$	COD
0	$1.0031 \pm 0.0022$	0.9944
1	$0.9998 \pm 0.0018$	0.9979
1.5	$1.0012 \pm 0.0023$	0.9951
1.9501	$0.856 \pm 0.051$	0.9984
1.9655	$0.44 \pm 0.56$	0.9998

Table 2: Values of  $\tau_C$  and the coefficient of determination obtained from the Boltzmann fit applied to the refinement region.

occurs exactly at

$$\left. \frac{dS}{d\tau} \right|_{\tau_C} = \frac{A_2 - A_1}{4\sigma_\tau}.$$

Moreover, by computing

$$\frac{d^2S}{d\tau^2} = \frac{(A_2 - A_1) \left( e^{\frac{\tau - \tau_C}{\sigma_\tau}} - e^{2\frac{\tau - \tau_C}{\sigma_\tau}} \right)}{\sigma_\tau^2 \left( 1 + e^{\frac{\tau - \tau_C}{\sigma_\tau}} \right)^3},$$

we observe that for  $\tau = \tau_C$  one has  $\frac{d^2S}{d\tau^2} = 0$ , showing that this point is indeed an inflection point.

The fit yields, with a coefficient of determination COD = 0.9976, the values  $A_1 = 165.6 \pm 0.03$ ,  $A_2 = 166.7 \pm 0.03$ ,  $\sigma_\tau = 0.033 \pm 0.002$ , and  $\tau_C = 0.9998 \pm 0.0019$ , which indeed includes  $\tau_C = \frac{T}{T_C} = 1$  within the confidence interval.

We repeat the same procedure for other values of  $D$  in the refinement region, as shown in Fig. 4(b). A good Boltzmann fit is obtained for  $D = 0$  and  $D = 1.5$ , exactly as observed for  $D = 1$ , with the confidence interval again containing  $\tau_C = \frac{T}{T_C} = 1$ . This is not the case for the point near the tricritical value nor for the tricritical point itself. The fitting results are summarized in Table 2. Notably, we obtain  $\tau_C \approx 1$  for points far from the tricritical point. On the other hand, the results show that the sigmoidal fit is not appropriate for points close to the tricritical region.

### 3.2. Random matrices theory

We now complete our analysis by examining the results in the framework of random matrix theory (RMT). In this part, we do not aim to locate the critical temperature; instead, we investigate how temperature affects the density of eigenvalues and the spacing distribution.

We begin by analyzing the eigenvalue density of the adjacency matrices of the VGs constructed for different anisotropies  $D$ . For simplicity, we focus on the cases  $D = 0$ ,  $D = 1$ , and the tricritical point. The results are shown in Fig. 5(a), (b), and (c), respectively.

We observe a tendency in which lower temperatures correspond to heavier tails in the eigenvalue density. Although the density of states appears to behave similarly at the critical and tricritical points, clear differences emerge at low temperatures. This can be seen in Fig. 5(d), where we illustrate the case  $T = 0.2T_C$  for both a critical point ( $D = 0$ ) and the tricritical point.

In the same panel, we also observe that at high temperatures both cases tend to approach the density of states obtained from uncorrelated Gaussian noise (represented by the gray line).

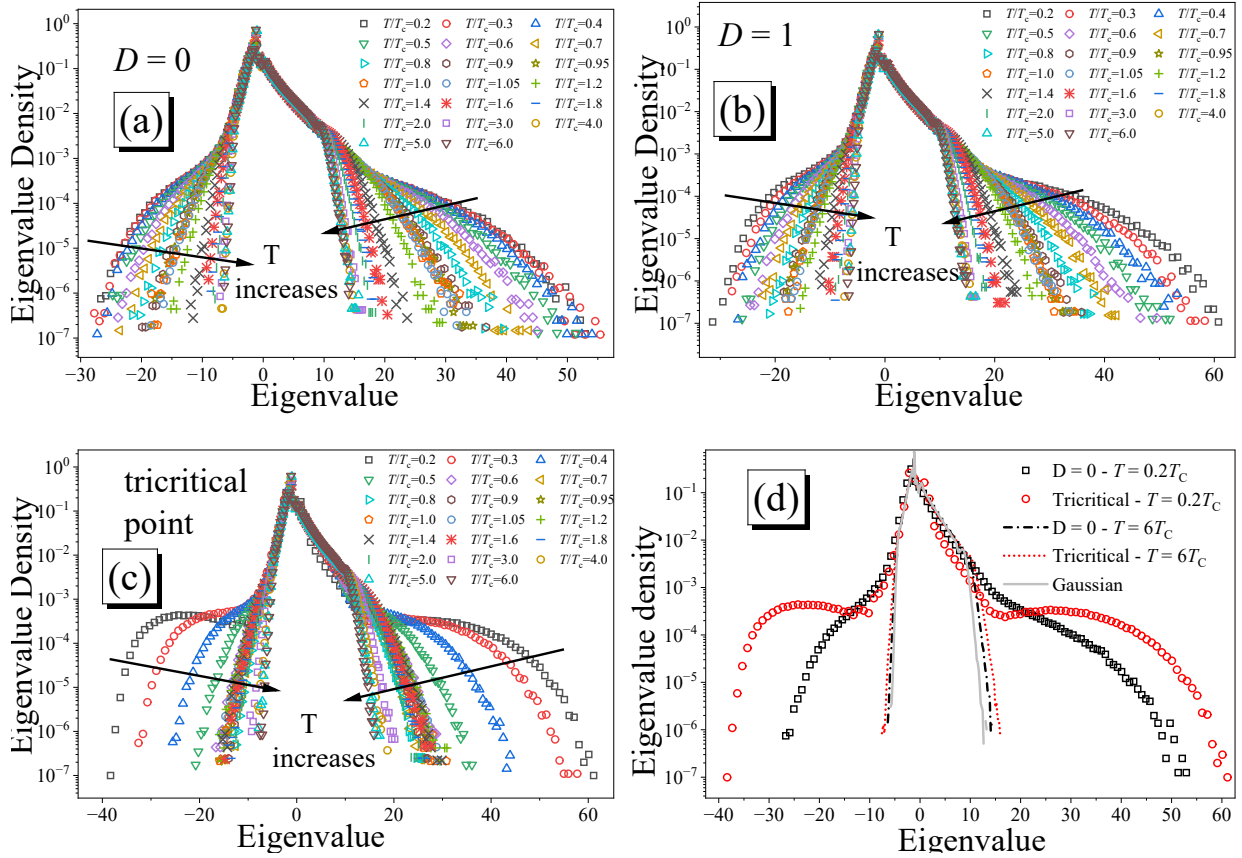


Figure 5: Density of eigenvalues of the adjacency matrix of the VGs for different temperatures. Panels (a) and (b) correspond to critical points, while panel (c) corresponds to the tricritical point. Panel (d) shows a comparison between the critical and tricritical cases at low and high temperatures, together with the eigenvalue density of a visibility graph obtained from uncorrelated Gaussian noise.

The gray curve is clearly not the semicircle law; rather, it corresponds to a stable law obtained when deriving the density of states of adjacency matrices of VGs constructed from uncorrelated Gaussian noise. To the best of our knowledge, there are no results in the literature describing stable laws for the eigenvalue density of VGs, suggesting that this point deserves further investigation.

Finally, it is important to note that the spectrum at the critical temperature exhibits, as expected, an intermediate tail between the low-temperature (longer tails) and high-temperature (shorter tails) regimes.

Next, we focus on the spacing distribution in order to investigate the effects of temperature for fixed anisotropies. We first order the eigenvalues and then compute histograms of the spacings  $s = \frac{\lambda_i - \lambda_{i-1}}{D}$ , with  $i = 2, \dots, N_{\text{steps}}$ . We begin by considering an anisotropy far from the tricritical point ( $D = 1.5$ ), as shown in Fig. 6(a).

Here the same pattern observed for the eigenvalue density is also established: longer tails correspond to low temperatures, while shorter tails correspond to high temperatures, which tend to approach the spacing distribution of the VG constructed from uncorrelated Gaussian noise (gray line). The critical temperature corresponds to an intermediate tail.

At this point it is useful to consider a simple and interesting ratio proposed by Oganessian and Huse [25]:

$$\tilde{r}_n = \frac{\min(s_n, s_{n-1})}{\max(s_n, s_{n-1})} = \min\left(r_n, \frac{1}{r_n}\right)$$

where

$$r_n = \frac{s_n}{s_{n-1}}$$

with  $s_n = \lambda_{n+1} - \lambda_n$ . This quantity does not require unfolding because ratios of consecutive level spacings are independent of the local density of states. Therefore, it allows a simpler comparison with experiments than the traditional level-spacing distribution [26]. We plot  $\tilde{r}$  as a function of  $T/T_C$  for the case  $D = 1.5$  in Fig. 6(b). The results are presented on a semi-log scale.

We observe that the values of  $\langle \tilde{r} \rangle$  range from approximately 0.468 up to slightly above 0.48. It is interesting to compare these values with those obtained for standard random-matrix ensembles. For example, for the Poisson ensemble the distribution of  $\tilde{r}$  is given by

$$P(\tilde{r}) = \frac{2}{(1 + \tilde{r})^2}$$

for  $0 \leq \tilde{r} \leq 1$ , and zero otherwise, which leads to

$$\langle \tilde{r} \rangle_{\text{Poisson}} = 2 \int_0^1 \frac{\tilde{r}}{(1 + \tilde{r})^2} d\tilde{r} = 2 \ln 2 - 1 \approx 0.3863.$$

On the other hand, the random-matrix ensembles GOE, GUE, and GSE (Gaussian orthogonal, unitary, and symplectic ensembles), corresponding to  $\beta = 1, 2$ , and  $4$ , lead to the distribution (see Atas *et al.* [26])

$$P(\tilde{r}) = C_\beta \frac{(\tilde{r} + \tilde{r}^2)^\beta}{(1 + \tilde{r} + \tilde{r}^2)^{1 + \frac{3}{2}\beta}}$$

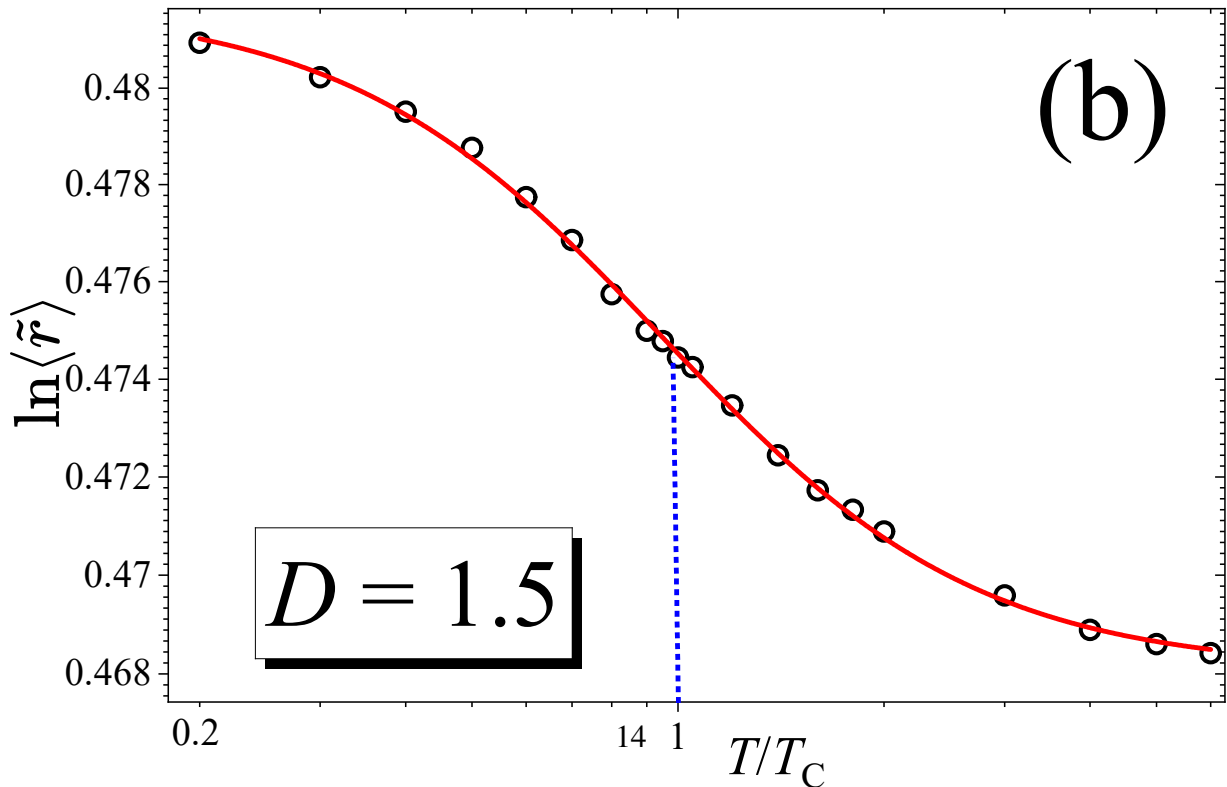
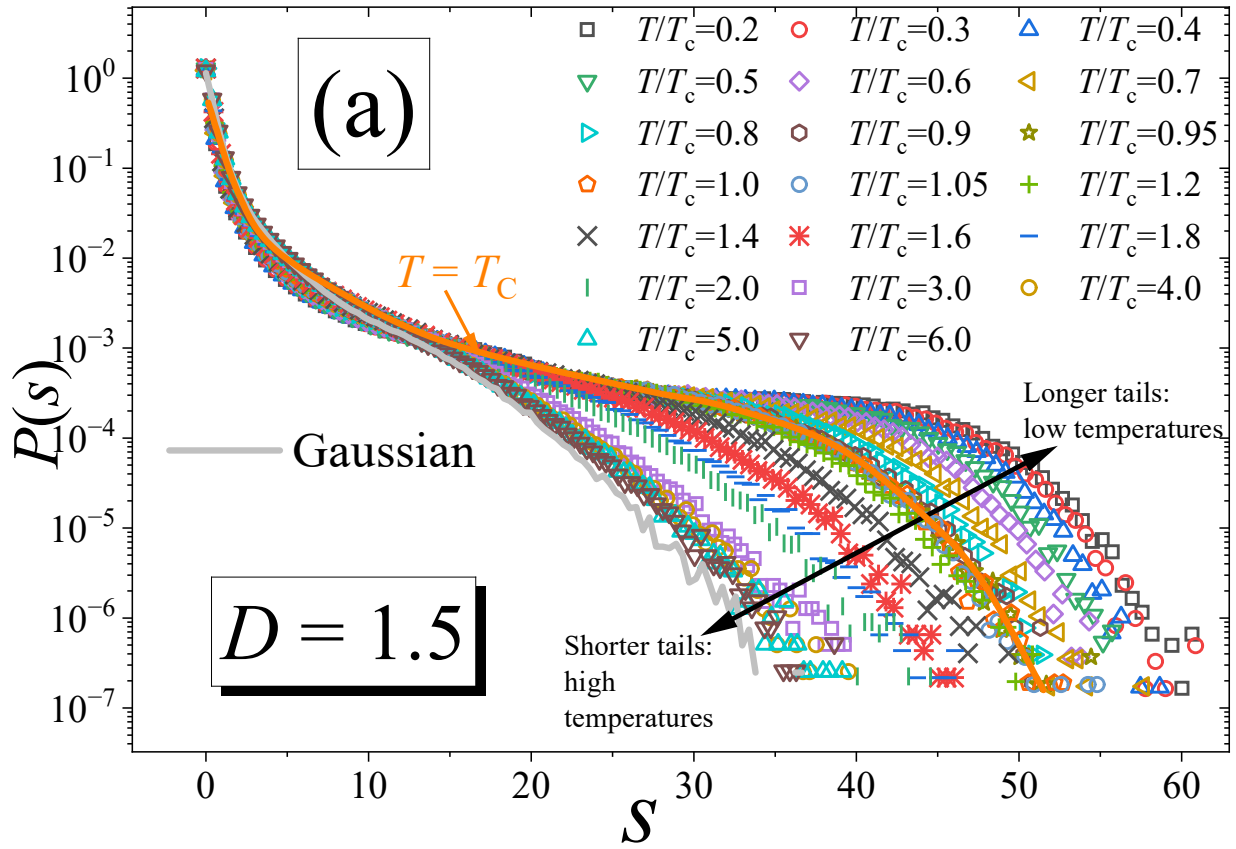


Figure 6: Spacing distribution of the eigenvalues of adjacency matrices of VGs. (a) Spacing distribution for  $D = 1.5$ . (b) Average value of  $\tilde{r}$  for  $D = 1.5$  as a function of  $T/T_c$ , which can be used instead of the spacing distribution.

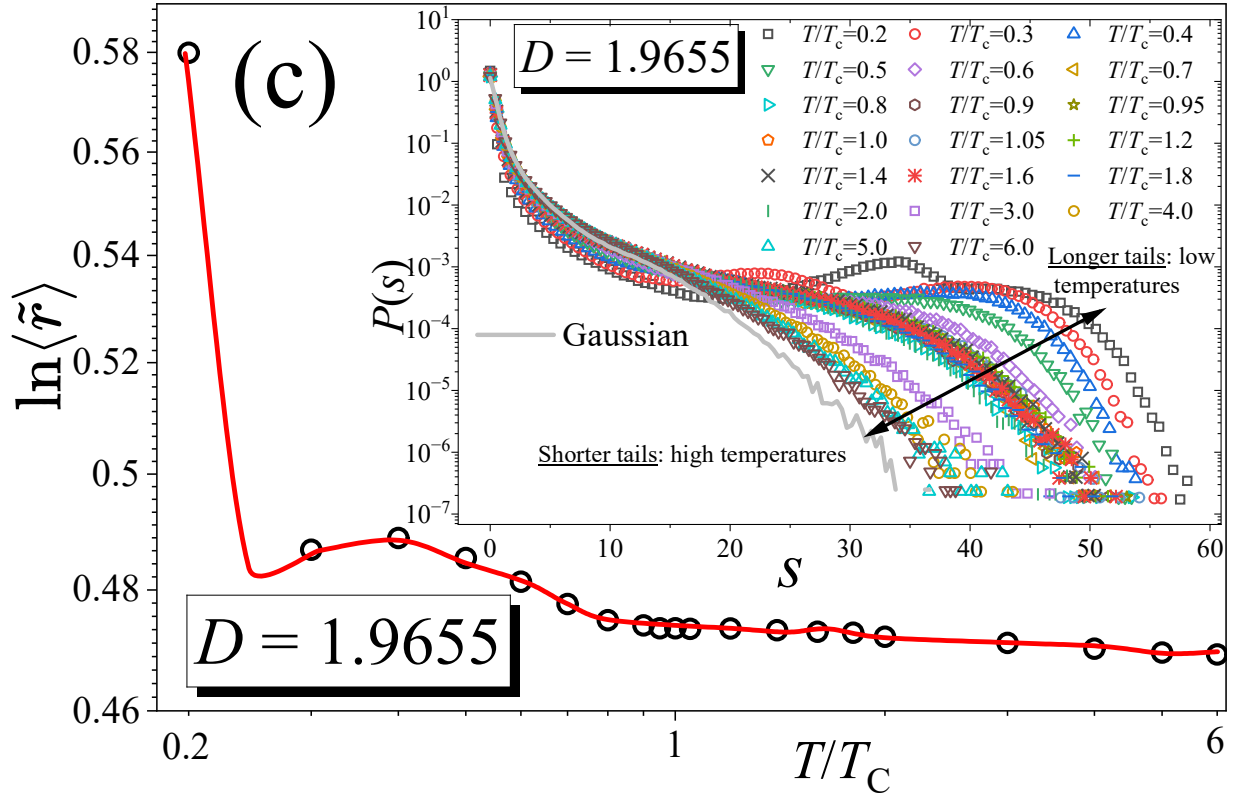


Figure 7:  $\langle \tilde{r} \rangle$  for the tricritical point as a function of  $T/T_C$ . The inset shows the corresponding spacing distribution for this point.

for  $0 \leq \tilde{r} \leq 1$ , and zero otherwise, where  $C_\beta$  is the normalization constant. The corresponding mean values are

$$\langle \tilde{r} \rangle_{\beta=1} = 4 - 2\sqrt{3} \approx 0.5359,$$

$$\langle \tilde{r} \rangle_{\beta=2} = \frac{2\sqrt{3}}{\pi} - \frac{1}{2} \approx 0.6027,$$

and

$$\langle \tilde{r} \rangle_{\beta=4} = \frac{32\sqrt{3}}{15\pi} - \frac{1}{2} \approx 0.6762.$$

Therefore, the values obtained at the critical point lie between those predicted for the Poisson and GOE ensembles. The same behavior is observed for the other critical points studied in this work, namely  $D = 0$  and  $D = 1$ .

On the other hand, for the tricritical point at low temperatures we observe a slight increase in  $\langle \tilde{r} \rangle$ , reaching  $\langle \tilde{r} \rangle \approx 0.58$ , which is larger than  $\langle \tilde{r} \rangle_{\beta=1}$  but still smaller than  $\langle \tilde{r} \rangle_{\beta=2}$ , as shown in Fig. 7.

For  $T \rightarrow \infty$ , we obtain  $\langle \tilde{r} \rangle_\infty \approx 0.468$  for both the critical and tricritical cases. This value corresponds to the spacing distribution of the spectrum of a VG constructed from uncorrelated Gaussian noise. The inset shows the spacing distribution for the tricritical case, highlighting the anomalous behavior observed at low temperatures.

#### 4. Summaries, conclusions, and discussions

We present a study of the universality of the Blume–Capel (BC) model by using spectral properties of visibility graphs (VGs) constructed from time series generated by Monte Carlo simulations. First, we calculate the eigenvalues of the Laplacian to show that the logarithm of the number of spanning trees of the visibility graphs (tree entropy, or structural entropy as we called it in [17]) is a good identifier of critical phenomena and of the crossover effects present in this model.

For this purpose, it is necessary to calculate the derivative of this quantity, which presents a pronounced peak at the critical temperature for points far from the tricritical point. Alternatively, a refinement of the region of structural entropy where the critical temperature is located indicates a good fit with a Boltzmann function, showing that the inflection point occurs exactly at  $T = T_C$ .

In a second analysis, we study the eigenvalue density and the spacing distribution of the adjacency matrices of the VGs generated by the Monte Carlo evolutions. Such an analysis illustrates that at high temperatures both the density and the spacing distributions exhibit shorter tails, whose limit ( $T \rightarrow \infty$ ) corresponds to the spectrum of a visibility graph generated from uncorrelated noise. At low temperatures, correlations lead to longer tails.

By using the interesting ratio  $\tilde{r}$  proposed by Oganesyanyan and Huse, which condenses the information of the spacing distribution, we show that the average value  $\langle \tilde{r} \rangle$  lies between the values predicted for the Poisson and the Gaussian orthogonal ensemble (GOE). However, the crossover effects drastically modify the behavior at low temperatures, where the average ratio surpasses the GOE value. At high temperatures, this statistic corroborates the limit  $\langle \tilde{r} \rangle_\infty \approx 0.468$ , corresponding to the spectrum of a VG constructed from uncorrelated Gaussian noise.

Although initially applied to the Ising model [17], and here extended with several additional results to cover the nuances of the BC model (an Ising model with spin 1 and anisotropy), the method can be applied to time series from a variety of problems to localize critical behavior in phenomena where the Hamiltonian is not known, such as climate, financial, epidemic time series, chaotic systems, and others. We believe that this powerful method can point to important directions and lead to new discoveries in complex systems.

#### Acknowledgements

R. da Silva acknowledges the financial support of CNPq under grants 304575/2022-4 and 406820/2025-2. This research was carried out with the support of the high-performance computing resources provided by the Information Technology Superintendence of the University of São Paulo and by the Lovelace Cluster at IF-UFRGS, Brazil.

#### References

- [1] M. Blume, V. J. Emery, R. B. Griffiths, Ising Model for the  $\lambda$  Transition and Phase Separation in  $^3\text{He}$ - $^4\text{He}$  Mixtures, *Phys. Rev. A* **4**, 1071–1077 (1971)

- [2] M. Blume, Theory of the First-Order Magnetic Phase Change in UO<sub>2</sub>, *Phys. Rev.* **141**, 517–524 (1966)
- [3] H. W. Capel, On the possibility of first-order phase transitions in Ising systems of triplet ions with zero-field splitting I and II, *Physica* **32**, 966–988 (1966), **33**, 295–314 (1967)
- [4] D. Mukamel, and M. Blume, Critical behavior of the Blume–Emery–Griffiths model, *Phys. Rev. A* **10**, 610–616 (1974)
- [5] A. N. Berker, M. Wortis, Blume–Emery–Griffiths–Potts model in two dimensions, *Phys. Rev. B* **14**, 4946–4963 (1976)
- [6] I. D. Lawrie and S. Sarbach, Theory of Tricritical Points, in *Phase Transitions and Critical Phenomena*, Vol. 9, edited by C. Domb and J. L. Lebowitz, Academic Press, London, 1984.
- [7] R. da Silva, N. A. Alves, e J. R. Drugowich de Felício, Universality and scaling study of the critical behavior of the two-dimensional Blume–Capel model in short-time dynamics, *Phys. Rev. E* **66**, 026130 (2002)
- [8] R. da Silva, Exploring the similarities between mean-field and short-range relaxation dynamics of spin models, *Braz. J. Phys.* **52**, (2022).
- [9] R. da Silva, Numerical evidence of Janssen-Oerding’s prediction in a three-dimensional spin model far from equilibrium, *Phys. Rev. E* **105**, 034114-1–034114-6 (2022)
- [10] R. da Silva, Random matrices theory elucidates the nonequilibrium critical phenomena, *Int. J. Mod. Phys. C* **34**, 2350061-1–2350061-12 (2023)
- [11] R. da Silva, E. Venites F., S. D. Prado, J. R. Drugowich de Felício, Efficient Computational method using random matrices describing critical thermodynamics, *Int. J. Mod. Phys. C* **37**, 2450163-1–2450163-24 (2024)
- [12] E. Venites F., R. da Silva, J. R. Drugowich de Felício, A Spectral Investigation of Criticality and Crossover Effects in Two and Three Dimensions: Short Timescales with Small Systems in Minute Random Matrices, *Entropy* **26**(5), 395 (2024)
- [13] L. Lacasa, , B. Luque, F. Ballesteros, J. Luque, J. C. Nuño, From time series to complex networks: the visibility graph, *PNAS* **105**(13), 4972–4975(2008)
- [14] L. Zhao, W. Li, C. Yang, J. Han, Z. Su, Y. Zou, A new method for characterizing time series based on visibility graphs, *PLoS ONE* **12**(1), e0170467 (2017)
- [15] D. Gómez-Hernández , D. García-Gudiño, E. Landa , I. O. Morales , A. Frank, Characterization of time series using visibility graphs: A comparative study, *PLOS ONE* **14**(9): e0221674 (2019).
- [16] J. T. Moraes, S. C. Ferreira, Visibility graphs for absorbing-state phase transitions, *Phys. Rev. E* **108**, 044309 (2023)

- [17] R. da Silva, H. A. Fernandes, P. G. Freitas, S. Gonçalves, E. V. Stock, A. Alves, The number of spanning trees as an indicator of critical phenomena: When Kirchhoff meets Ising, *Phys. Rev. E* (accepted for publication) <https://doi.org/10.1103/kzxs-9pv8> (2026)
- [18] B. Bollobás, *Modern Graph Theory*, Springer, 1998.
- [19] R. Diestel, *Graph Theory*, 5th ed., Springer, 2017
- [20] R. P. Stanley, *Enumerative Combinatorics*, Vol. 2, Cambridge University Press, 1999.
- [21] G. Kirchhoff, On the solution of the equations to which one is led in investigating the linear distribution of galvanic currents, *IRE Trans. Circuit Theory*, **5**(1), 4–7 (1958), translated by J. B. O’Toole from the original in German: Über die Auflösung der Gleichungen, auf welche man bei der Untersuchung der linearen Verteilung galvanischer Ströme geführt wird, *Annalen der Physik und Chemie*, **72**, 497–508 (1847).
- [22] Frank Harary, *Graph Theory*, Addison-Wesley, Reading, Massachusetts, 1969.
- [23] P. Butera, M. Pernici, The Blume–Capel model for spins  $S = 1$  and  $3/2$  in dimensions  $d = 2$  and  $3$  *Physica A* **507**, 22–66 (2018)
- [24] P.D. Beale, Finite-size scaling study of the two-dimensional Blume–Capel model, *Phys. Rev. B* **33**, 1717–1720 (1986)
- [25] V. Oganessian, D. Huse, Localization of interacting fermions at high temperature, *Phys. Rev. B* **75**, 155111-1–155111-5 (2007)
- [26] Y.Y. Atas, E. Bogomolny, O. Giraud, G. Roux, *Phys. Rev. Lett.* **110**, 084101-1–084101-5 (2013)